

# Flow Prediction of Complex Fluids in a Circular Pipe by Utilizing a Velocity-Profiling-Assisted Rheometer

Kohei Ohie,\* Taiki Yoshida, Yuji Tasaka, and Yuichi Murai



Cite This: *Ind. Eng. Chem. Res.* 2022, 61, 18157–18164



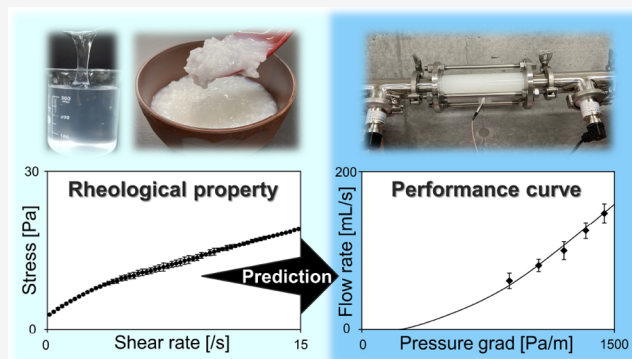
Read Online

ACCESS |

Metrics & More

Article Recommendations

**ABSTRACT:** Flow prediction of complex fluids in a circular pipe was conducted using a velocity-profiling-assisted rheometer. As application examples, shear-rate-dependent stress and viscosity of carboxymethyl cellulose and polyacrylamide aqueous solutions and rice porridge were evaluated. Carboxymethyl cellulose is a well-known thickener for foods and cosmetics; the latter two examples represent complex fluids that are outside the scope of application of a standard torque-type rheometer because the PAM solution causes shear-localization problems and the porridge includes  $O(1\text{ mm})$  size dispersions. The obtained flow curve in shear rate range of  $O(10^{-1}–10^1\text{ s}^{-1})$  was used to predict laminar flow in a pipe under a steady pressure gradient, which is an industrially applicable target. The predicted velocity profiles were in good agreement with experimental results measured in a pilot pipeline, where the maximum relative error of flow rate was less than 10% for all test fluids. This suggests that the application of the rheological evaluation to flow prediction has high industrial practicality to complex fluids which are out of application of the standard rheometer.



## INTRODUCTION

Prediction of flows of foods and chemical products plays an important role in the optimal design and efficient control of production lines in industrial fields. In the design process, for example, relationships between pressure loss and flow rate through an entire pipeline enable reasonable selections of driving pumps and pressure sensors without relying solely on so-called “rules of thumb” or related prior experience. The target fluid is usually non-Newtonian. Such fluid applications are diverse and complex, ranging from highly functional foods to transport of coal slurries for effective utilization of fossil resources. Simulation of non-Newtonian fluid flow requires a constitutive equation that can properly represent its rheological properties. In the past century of rheology history, there have been countless constitutive equations proposed, based on both theoretical and empirical approaches.<sup>1–3</sup> A representation of the former is the FENE-P model,<sup>4,5</sup> which originates from a spring–beads model that simulates viscoelasticity of a polymer constituent. This is widely used for predicting flows of dilute polymer solutions in various geometries from laminar to turbulent conditions.<sup>6,7</sup> Parameters included in the models are usually identified from shear test data that are measured by a standard torque-type rheometer.

This customary procedure, however, encounters problems in industrially practical targets, such as foods and chemical products. A standard torque-type rheometer assumes a constant apparent shear rate in its narrow fluid layer, and the

corresponding shear stress is indirectly evaluated from the integrated axial torque.<sup>8,9</sup> In cases of some polymer solutions, such as that of polyacrylamide, this basic assumption is faulty owing to shear-banding within a narrow gap.<sup>10–13</sup> Evaluated rheological properties would then include bias errors,<sup>14,15</sup> and accurate flow prediction cannot be performed using a rheological model identified with such poor data. Despite increasing demands from industrial fields, heterogeneous fluids, such as foods that are swallowed and coal slurries, which contain  $O(1\text{ mm})$  size ingredients or dispersions, are also immediately out of scope because the fluids do not fit within the millimeter gap at most.<sup>16</sup> Laminar flow data truly obtained with a standard torque-type rheometer can be used to predict, for example, laminar behavior in a circular pipe. But its target fluid is limited to relatively simple fluids such as dilute polymer solutions because of the above problems.

One way to identify rheological properties is by using a theoretical approach, which starts with modeling of internal structures; a relationship between bulk shear stress and shear

**Received:** August 23, 2022  
**Revised:** November 18, 2022  
**Accepted:** November 18, 2022  
**Published:** December 1, 2022



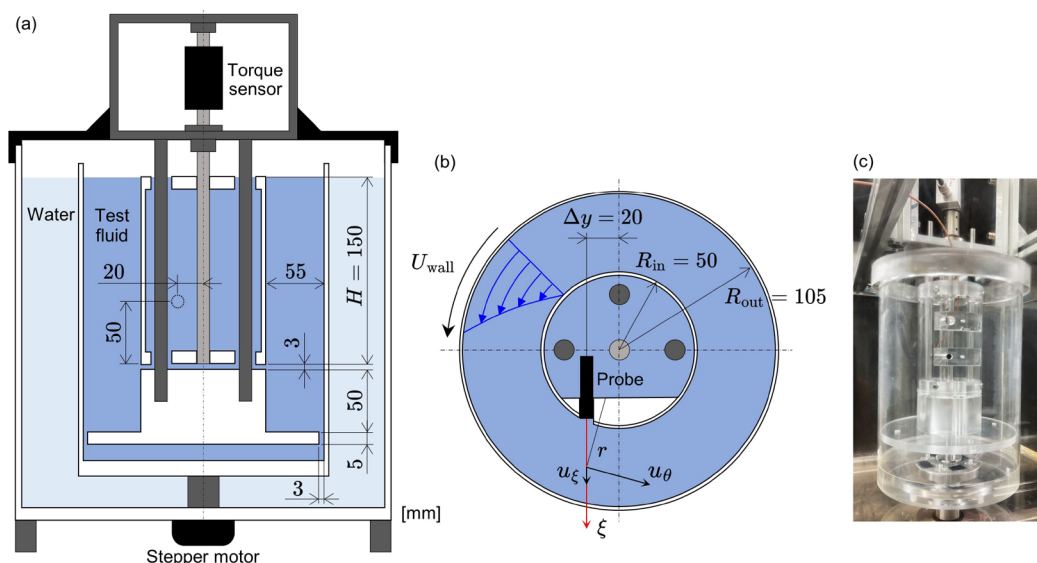


**Figure 1.** Schematics of a rheometer combined with ultrasonic velocity profiling for evaluating shear-rate-dependent rheological properties of complex fluids: (a) vertical cross-sectional view, (b) horizontal cross-sectional view at the height of the ultrasonic probe, and (c) photograph of rheometer taken from the side, in which the test fluid and surrounding water are not present for better visibility. Unit of length: mm.

rate is derived based on fluid mechanics. For example, determination of the effective viscosity of solid particle and bubble suspensions, mainly by volcanologists, has a long history and these parameters have almost been revealed under steady shear conditions.<sup>17–20</sup> From a viewpoint of industrial application, however, the theoretical approach is not practical for construction of constitutive equations of fluid products with various individual characteristics. A more versatile approach is to obtain rheological properties based on an actual shear test in a laboratory. Owing to the applicable limitations of the standard rheometer with respect to complex fluids, Derakhshandeh et al. developed a novel torque-type rheometer combined with ultrasonic velocity profiling.<sup>21–23</sup> Compared with other velocimetry techniques such as particle imaging velocimetry (PIV), UVP has prominent advantage for opaque fluids and multiphase fluids like rice porridge examined in the present study. Specifications of comparison with other techniques such as magnetic resonance imaging (MRI) velocimetry are summarized in our previous paper.<sup>24</sup> The velocity-profiling-assisted rheometer allows for spatial variations of shear stress and shear rate within the gap between double concentric cylinders, so shear-localization problems are not encountered. Spatial profiles of shear stress and shear rate are determined by measuring velocity distributions and axial torque acting on the inner cylinder. Local evaluation of rheology of complex fluids within the vessel itself has high potential: this instrument is considered pioneering technology for velocity-profiling-assisted rheometers.

The purpose of this study was to predict laminar shear flows of complex fluids using shear viscosity data obtained by the velocity-profiling-assisted rheometer. It is shown that introduction of this rheometer greatly expands the range of fluid targets for which flow prediction is possible. To explore applicability of the method to industrially practical targets in chemical and food engineering, demonstrations were conducted with representative complex fluids, such as a polyacrylamide aqueous solution and a porridge containing  $O(1\text{ mm})$  size rice grains. The obtained rheological properties were utilized to predict one-directional fluid flows in a circular

pipe under a constant pressure gradient. This is a basic geometry but of most industrial importance. The predictions are compared with experimental results measured in a pilot pipeline system. Validity of the extrapolation from rheological characterization to flow prediction is examined.

## ■ RHEOLOGICAL EVALUATION

**Velocity-Profiling-Assisted Rheometer.** Schematics and a photograph of the rheometer combined with an ultrasonic velocity profiler (UVP) are shown in Figure 1. The instrument consists of a fixed inner cylinder of  $R_{in} = 50\text{ mm}$  connected to an axial torque sensor (UTMIII, 0.5 N m, Unipulse Co., Ltd., Japan) and an outer cylinder of  $R_{out} = 105\text{ mm}$  driven by a stepper motor with a constant rotation speed. Under this configuration, azimuthal one-directional flow is realized between the double concentric cylinders, as schematically shown in Figure 1b. The maximum shear rate realized in this prototype is  $O(10^1\text{ s}^{-1})$  with assumptions of a Newtonian fluid and maximum rotation speed of 50 rpm. This is lower than that of a standard torque-type rheometer because of the wide gap between the double cylinders. Expansion of the shear rate range is possible to  $O(10^2\text{ s}^{-1})$  by narrowing the gap and increasing the maximum rotation speed of the stepping motor. Note that it was mainly focused on obtaining shear-rate-dependent stress for predicting pipe flows. The rheological evaluation in the wide range is therefore not necessary for the prediction, where the maximum shear rate is  $O(10^1\text{ s}^{-1})$  at most in a pilot pipeline appearing in a later section. A stepped cylinder is suspended by three stainless rods from the base and placed under the inner cylinder to insulate the influence of secondary flow, that is, end effects induced by the bottom of the outer cylinder. Neither the stepped cylinder nor rods are in contact with the inner cylinder, so the torque sensor measures axial torque that is caused solely by simple shear stress acting on the inner cylinder wall. This is an improvement over the velocity profiling-assisted rheometer described in previous studies,<sup>21,25,26</sup> which simply consisted of inner and outer cylinders. This experimental apparatus is, nevertheless, a prototype and therefore has some shortcomings, such as its

large size and the fact that the inner cylinder is also filled with the test fluid. A large amount of test sample is required compared with a standard torque-type rheometer. This size problem can be solved by minimizing the height and gap-size; the amount of a test fluid will be reduced to 500 mL, which will be improved in the next version.

The ultrasonic probe of an UVP (UVP Duo monitor, MetFlow SA, Switzerland) is horizontally inserted into the inner cylinder at an off-axis position of  $\Delta y = 20$  mm to capture the azimuthal velocity profile  $u_\theta(r, t)$ . Frequency of the ultrasonic wave was 4 MHz and the active diameter of the probe was 5 mm. As shown in Figure 1b, the UVP captured spatiotemporal distribution of velocity components in the propagation direction of the ultrasonic waves. Spatial resolution of the UVP was approximately 1 mm in the propagation direction, and its temporal resolution was  $O(10$  ms). The UVP measurement volume was therefore a cylinder with a diameter of 5 mm and height of 1 mm. The higher the emission frequency is, the better spacial resolution UVP has, but the ultrasonic pulse is attenuated more. For example, clay suspensions with volume fraction of 30 wt % can be measured by a low emission frequency 2 MHz transducer: application range of the velocity-profiling-assisted rheometer is wide. Assuming that flow in the gap is axisymmetric and dominates in the azimuthal direction,  $u_\xi(\xi, t)$  is uniquely converted to  $u_\theta(r, t) = (r/\Delta y)u_\xi(\xi, t)$ . When the outer cylinder rotates with a constant azimuthal velocity  $U_{\text{wall}}$ , spatial distributions of simple shear rate are obtained from the averaged velocity profile  $\bar{u}_\theta(r)$  as

$$\dot{\gamma}(r) = \left( \frac{d}{dr} - \frac{1}{r} \right) \bar{u}_\theta(r) \quad (1)$$

Synchronously with the UVP measurement, the torque sensor measures the temporal profile of the axial torque  $T(t)$  acting on the inner cylinder. Shear stress acting on the inner cylinder is therefore obtained from the time-averaged axial torque  $T$  as

$$\tau_{\text{wall}} = \frac{T}{2\pi R_{\text{in}}^2 H} \quad (2)$$

where  $H$  is height of the inner cylinder, as shown in Figure 1a. Considering conservation of angular momentum, the spatial profile of shear stress is derived as

$$\tau(r) = \tau_{\text{wall}} \left( \frac{R_{\text{in}}}{r} \right)^2 \quad (3)$$

Shear-rate-dependence of shear stress  $\tau(\dot{\gamma})$ , generally called a flow curve, was obtained by combining eqs 1 and 3. For improving precision of the evaluation, dozens of flow curves are obtained by increasing rotation speed of the outer cylinder gradually. Average shear stress at each  $\dot{\gamma}$  is evaluated in the range from  $\dot{\gamma} - \Delta\dot{\gamma}$  to  $\dot{\gamma} + \Delta\dot{\gamma}$  with  $\Delta\dot{\gamma} = 1 \text{ s}^{-1}$ , and corresponding standard deviations are also evaluated, which therefore also reflects precision of the shear rate calculated from the velocity data obtained by the UVP measurement.

A standard torque-type rheometer assumes a constant shear rate in its narrow gap. In cases of some polymer solutions, the evaluated rheological properties include bias errors caused by shear-localization problems. The velocity-profiling-assisted rheometer mitigates these problems and enables robust evaluation of complex fluids, including high-molecular-weight

polymer solutions and heterogeneous materials, as explained in the following section.

**Preparation of Test Fluids.** As application examples, four test fluids were examined using the velocity-profiling-assisted rheometer (see photographs in Figure 2). The first represented

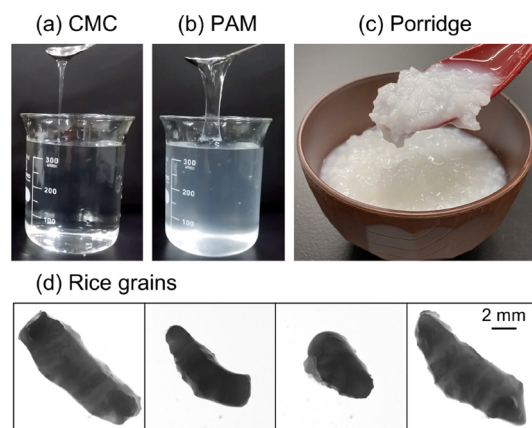


**Figure 2.** Photographs of (a) carboxymethyl cellulose (CMC) and (b) polyacrylamide (PAM) aqueous solutions, (c) rice porridge, and (d) photomicrographs of a rice grain in the porridge.

a Newtonian fluid: silicon oil (Shin-Etsu Chemical Co., Ltd., Japan) with a viscosity of 0.29 Pa·s. The second was carboxymethyl cellulose (CMC), as 0.8 wt % aqueous solution (CMC1190, Daicel Miraizu Ltd., Japan; Figure 2a) with molecular weight of  $8.2 \times 10^5$ . It has weak shear-thinning properties<sup>27–29</sup> and is used as a thickener for foods and cosmetics. The third test fluid was polyacrylamide (PAM), used as 0.8 wt % aqueous solution (Accofloc N-100S, MT AquaPolymer Co., Ltd., Japan; Figure 2b) with molecular weight of  $1.3 \times 10^7$ . The PAM solution has strong viscoelasticity and shear-thinning properties.<sup>30–32</sup> These characteristics make it unsuitable for standard torque-type rheometer measurements because of shear-localization problems, so the PAM solution is a challenging target for demonstrating applicability of the velocity-profiling-assisted rheometer. The fourth test fluid was rice porridge, as shown in Figure 2c. This is a well-known commercial item (TableMark Co., Ltd., Japan) in Japan. The original porridge with 300 mL of pure water added per liter was used in the experiments. The shape of the rice grains is almost an ellipsoid body having short axis of 5 mm and long axis of 10 mm at most, and they are wet as shown in Figure 2d. These rice grains were not separated, so this example represents a complex fluid that may not be measured correctly by a standard rheometer but for which there is high demand from the food and chemical industries.

A small amount of tracer particles (CL-2507, Sumitomo Seika Chemicals Co., Ltd., Japan) of 0.92 g/mL density and 180  $\mu\text{m}$  mean diameter was added to the silicon oil to serve as ultrasonic reflectors for the UVP measurements. For the CMC and PAM solutions, different particles (CHP20/P120, Mitsubishi Chemical Co. Ltd., Japan) of 1.01 g/mL density and 75–150  $\mu\text{m}$  mean diameter were used to satisfy the neutrally buoyant condition. As in the case of the silicon oil, 5 g of the tracer particles was added per 1 L of each solution. There was no need to add particles to the porridge because the rice grains themselves acted as ultrasonic reflectors. The temperature of the test fluids was kept at  $25.0 \pm 0.5$  °C in all

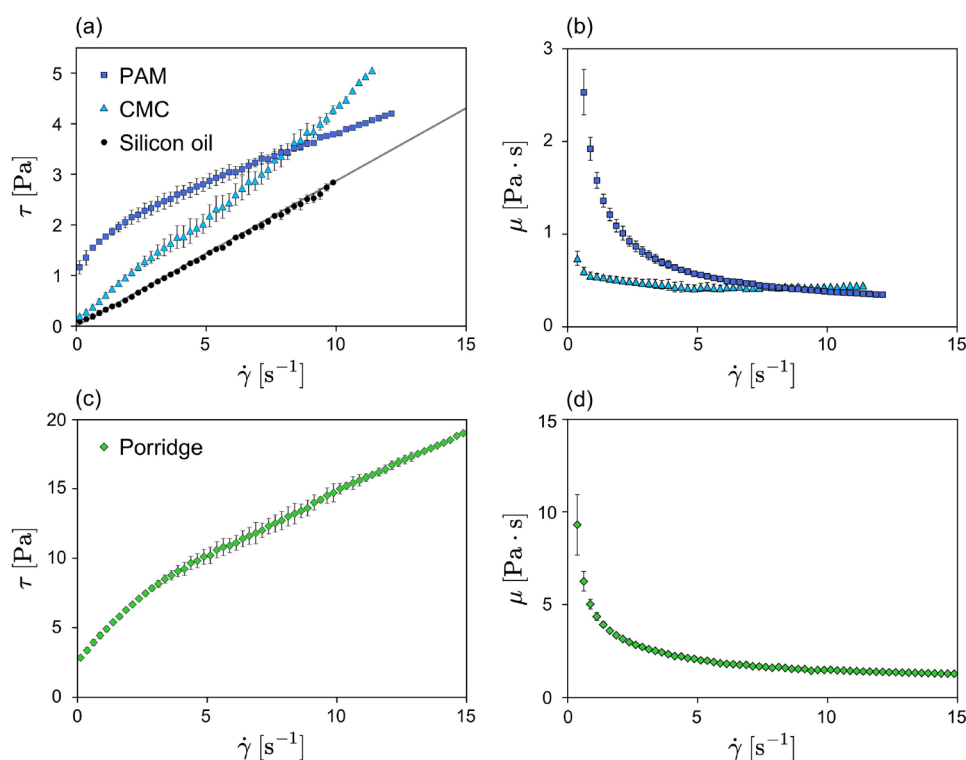


**Figure 3.** Rheological properties of test fluids examined by the velocity-profiling-assisted rheometer. (a) Flow curves of silicon oil and CMC and PAM solutions, where the solid line represents the flow curve of a Newtonian fluid with a viscosity coefficient of 0.29 Pa·s. Error bars represent standard deviations. (b) Viscosity curves of CMC and PAM solutions converted from the flow curves. (c) Flow curve and (d) converted viscosity curve of rice porridge.

experiments by use of a thermostatic chamber and air conditioning.

**Shear-Rate-Dependent Rheological Properties.** Rheological properties of the four test fluids were examined using the velocity-profiling-assisted rheometer. Rotation speed of the outer cylinder was gradually increased by 2 rpm from 0 to 40 rpm for the CMC and PAM solutions and from 0 to 50 rpm for the porridge. In each condition, axial torque and velocity measurements were conducted a minute after the rotation speed increased for ensuring the flow fully developed. The obtained flow curves were statistically analyzed as mentioned previously. Regarding instability limitation of the azimuthal flow between the double cylinders, the maximum Reynolds numbers of the outer and inner cylinders are  $Re_{out} = O(10^0)$  and  $Re_{in} = 0$ . The flow is therefore ensured as laminar Couette flow according to the flow regime map.<sup>33</sup>

Flow curves of the silicon oil and CMC and PAM solutions are summarized in Figure 3a. The solid line represents the flow curve of a Newtonian fluid with a viscosity of 0.29 Pa·s, which corresponds to the catalog value of the silicon oil. The flow curve of the silicon oil is consistent with the solid line, which validates measurements using this rheometer. The error bars of the silicon oil were shorter than those of other test fluids. As mentioned previously, the standard deviations also reflect precision of the shear rates calculated from the velocity distribution measured by the UVP. The quality of the velocity data of the silicon oil was better than others because the acoustic impedance difference of the solvent and tracer particles for the UVP measurement was the highest in all the test fluids.

In contrast to the silicon oil, the CMC and PAM solutions seemed to have finite values at the lowest shear rate, of  $0.20 \pm$

$0.02$  (standard deviation) Pa and  $1.16 \pm 0.13$  Pa, respectively. These are attributed to yield stresses; therefore, these fluids do not flow until a certain shear stress is applied. These flow curves were converted to viscosity curves, as shown in Figure 3b using the relationship of  $\mu = \tau/\dot{\gamma}$ . Viscosity of the solutions decreased as shear rate increased; i.e., these fluids exhibited shear-thinning properties. The PAM solution showed remarkable shear thinning because its molecular weight is much higher than that of the CMC solution. Shear-rate-dependent stress and viscosity of the porridge are shown in Figure 3c and Figure 3d, respectively. Yield stress and shear thinning properties are confirmed. The yield stress of  $2.83 \pm 0.09$  (standard deviation) Pa and viscosity were, however, much higher than those of the CMC and PAM solutions because the porridge contained rice grains at a volume fraction close to the packing limit. Flow curves were also obtained by decreasing rotation speed of the outer cylinder, but they matched with those in Figure 3; there are no thixotropic effects in the time scale of  $O(10$  min).

## FLOW PREDICTION IN A CIRCULAR PIPE

**Prediction Protocol.** A methodology for predicting a shear flow velocity profile in a circular pipe under a steady pressure gradient is briefly introduced. Assuming the flow is axially symmetric and dominates in one direction, as shown in Figure 4a, axial velocity  $u$ , shear stress  $\tau$ , and pressure gradient in the axial direction  $\alpha(t) = -\partial p/\partial x$  satisfy the following equation:<sup>34–36</sup>

$$\rho \frac{\partial u(r, t)}{\partial t} = \alpha(t) + \left( \frac{\partial}{\partial r} + \frac{1}{r} \right) \tau(r, t) \quad (4)$$

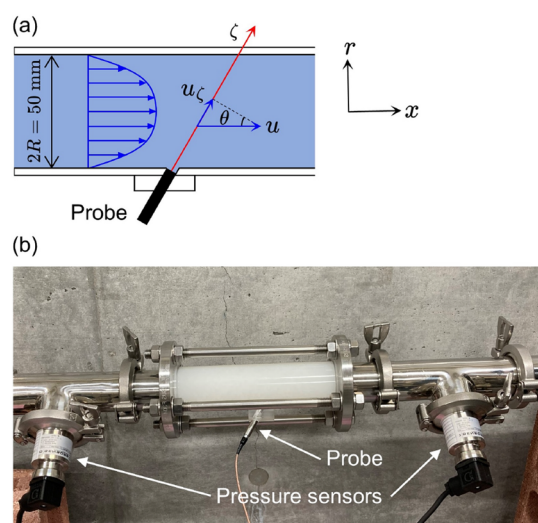


**Figure 4.** Pilot pipeline used for verification experiments: (a) schematic of a measurement section attached in pilot pipeline and geometric conditions for UVP measurement and (b) photograph of measuring unit in the pipeline, showing flow of the porridge as fluid.

where  $\rho$  is fluid density. Under a steady-state condition, i.e.,  $\partial/\partial t = 0$  and  $\alpha$  is constant, the spatial profile of the shear stress  $\tau(r)$  is determined from eq 4 independent of whether the fluid is Newtonian or non-Newtonian:<sup>37,38</sup>

$$\tau(r) = -\frac{\alpha r}{2} \quad (5)$$

The velocity-profiling-assisted rheometer provided the flow curves, as shown in Figure 3a and Figure 3c, so  $\tau(r)$  is uniquely converted to a spatial profile of shear rate  $\dot{\gamma}(r)$ . In axial flow, shear rate is defined as

$$\dot{\gamma}(r) = \frac{du}{dr} \quad (6)$$

Therefore,  $u(r)$  is obtained by integrating eq 6 under the boundary conditions of  $u(r = R) = 0$ , which reflects a nonslip condition on the pipe wall. This assumption is adopted because slip flow was not confirmed in all the velocity data measured in the velocity-profiling-assisted rheometer. In the case that slip condition at the wall is detected by the rheometer, the boundary condition has to be changed. The prediction protocol above assumes laminar shear flow and that the flow curve of the target fluid is unique with respect to applied shear rate.

**Experimental Setup for Validation.** A pilot pipeline was built in the laboratory for validation of this proposed prediction protocol. The experimental setup was a circulation circuit that connected a storage tank and rotary lobe pump with stainless pipes with an inner diameter of  $2R = 50$  mm. A test fluid in the tank was drawn to the pump through the pipe and returned to the tank through another pipe. Flow rate is roughly correlated with rotation speed of the pump. A photograph of a measuring unit attached to the returning pipe is shown in Figure 4b. The measuring unit was located more than 1.5 m apart from the rotary pump for ensuring that the flow is fully developed. Because one of the test fluids was opaque, UVP was suitable for measuring the spatial profile of the axial velocity  $u(r, t)$ . The ultrasonic transducer was installed at an angle of  $\theta = 30^\circ$  with respect to the direction

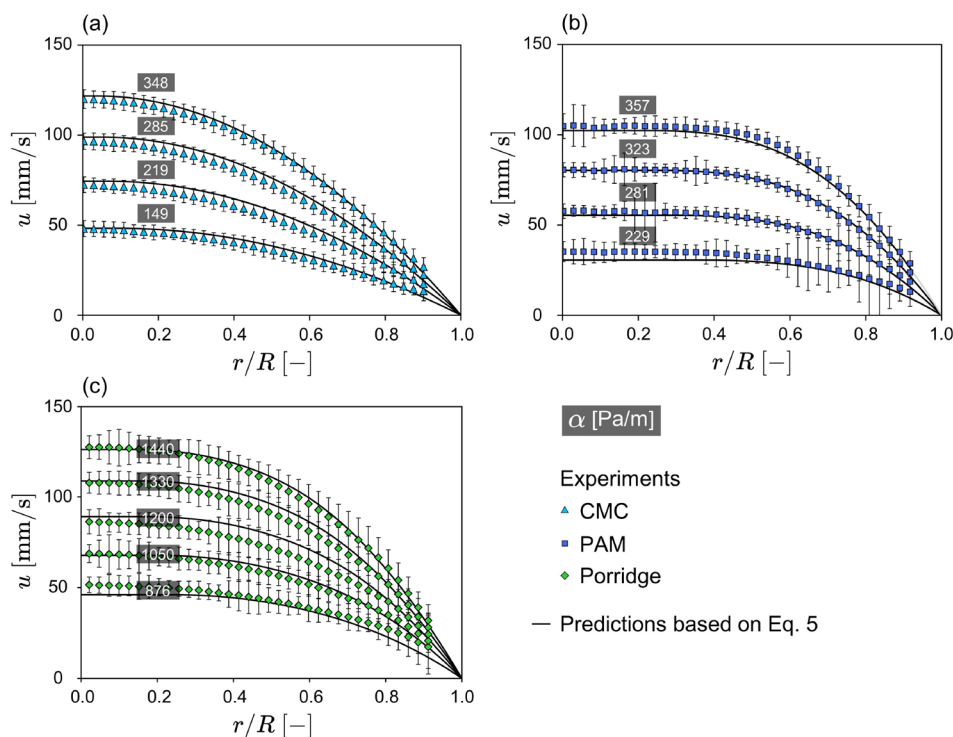


**Figure 5.** Comparison of predicted and measured results for (a) CMC, (b) PAM, and (c) porridge. Symbols are measured results obtained by UVP, where the error bars indicate standard deviations. Solid lines are predictions based on the rheological properties evaluated by the velocity-profiling-assisted rheometer. In the graph (b), radial range, where the velocity profile was predicted with the extrapolated flow curve, is shown with gray solid line. The numbers in white on each line indicate the pressure-gradient conditions.

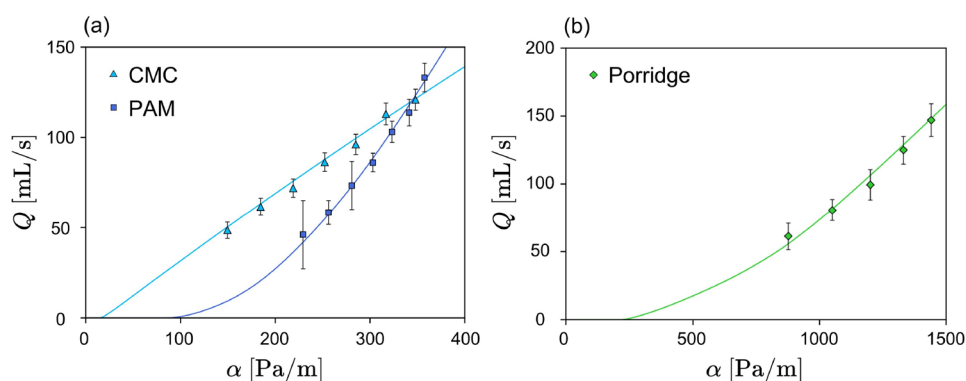


**Figure 6.** Pressure loss–flow rate relationships for (a) CMC and PAM solutions and (b) porridge. Solid lines and symbols are the respective predicted and experimental results obtained by integration of the velocity profiles shown in Figure 5. Error bars indicate 3 times the standard deviation.

perpendicular to the axial flow, as shown in Figure 4a. With assumptions of axial symmetry and one-directional flow, the velocity distribution  $u_\zeta(\zeta, t)$  captured by the UVP was converted to  $u(r, t)$  using the relationship of  $u = u_\zeta/\sin\theta$ . Synchronously with the velocity measurement, two pressure sensors (DMK351P, BD Sensors GmbH, Germany), installed on each side of the UVP section, were used to measure the pressure gradient. Predictions were compared with experimental results under the same pressure-gradient conditions.

#### Comparison of Predicted and Experimental Results.

Spatial profiles of the axial velocity were predicted under different pressure-gradient conditions based on the rheological properties obtained using the velocity-profiling-assisted rheometer as shown in Figure 5a–c with solid lines. As shown in Figure 3a,c, the maximum shear stresses are 5.1 Pa for the CMC solution, 4.2 Pa for the PAM solution, and 19.0 Pa for the porridge, and these correspond to the maximum pressure gradients obtained by eq 5, 408 Pa/m for the CMC solution, 336 Pa/m for the PAM solution, and 1520 Pa/m for the porridge. For the PAM solution, the flow curve was linearly extrapolated with a constant gradient identified in shear rate range of 6–12  $s^{-1}$  for predicting flows in higher pressure gradient conditions tentatively. The radial range, where the velocity profile was predicted with the extrapolated information, is shown with gray solid line in Figure 5b.

Corresponding experimental results are shown by symbols and error bars in Figure 5. The UVP measurement was conducted for each test fluid with time resolution of 25 ms for 3000 profiles. Average values and standard deviations were calculated at each radial position, which are shown by the symbols and error bars in Figure 5. Velocity information is lost close to the cylinder wall,  $r/R = 1.0$ , because this region includes the so-called near field, where the ultrasonic beam is not fully formed. Measurement precision of the porridge was statistically worse than that of the CMC and PAM solutions in the flow curves and velocity profiles in the circular pipe. This is attributed to precision of the UVP measurement. Acoustic impedance difference of solvent and tracer particles is higher in the case of the CMC and PAM solutions; quality of the velocity measurement data obtained by UVP was therefore better than those of the porridge. In addition, quality of the UVP measurement was blurred because of the attenuation of the ultrasonic pulses by the rice grains with a volume fraction close to the packing limit.

The lowest viscosity of the target fluids was  $O(0.1 \text{ Pa}\cdot\text{s})$ , as shown in Figure 3b, the corresponding velocity intensity in the pipe was  $O(100 \text{ mm/s})$ , as shown in Figure 5, and the pipe diameter, which is a representative length scale, was  $O(10 \text{ mm})$ , so the Reynolds number was  $O(10)$ . Therefore, use of eq 4, which assumes laminar flow, holds well. In addition, inlet length estimated with a well-known formula  $0.065 \text{ Re } D$  was  $O(0.1 \text{ m})$  at most, where  $D$  represents diameter  $2R = 50 \text{ mm}$ . The flow in the measuring unit was therefore fully developed.

Considering the measurement precision of the experiments, as shown by the error bars in Figure 5, the predictions are in good agreement with the measurement results for all cases of the three test fluids. The CMC solution had the lowest yield stress and weak shear thinning, so the velocity profiles are similar to parabolic shapes as shown in Figure 5a, i.e., Poiseuille flows. The PAM solution had relatively higher yield stress and strong shear thinning, so the profiles are flat near the center of the axis as shown in Figure 5b. These characteristic flow shapes were well reproduced by the predictions. More surprisingly, the predictions also worked well for the case of the rice porridge: similar to the PAM solution, this fluid had relatively high yield stress and strong shear thinning, so the velocity profiles were flat around the axis as shown in Figure 5c.

From the viewpoint of industrial application, it may be more attractive to estimate the relationship between pressure loss and flow rate. The flow rate  $Q$  was obtained from the velocity profiles in Figure 5 using the following integral operation:

$$Q = \int_0^R u(r)2\pi r \, dr \quad (7)$$

Velocity profiles were lost near the wall in the experiments because of the near field, so they were extrapolated in the radial direction using a nonslip assumption. The relationships between pressure gradient and flow rate are shown in Figure 6a for the CMC and PAM solutions, where the solid lines and symbols are the predicted and experimental results, respectively. In addition to the four conditions displayed in Figure 5a,b, the experimental results for another three pressure gradients were added, giving a total of seven conditions plotted in Figure 6a for each solution. Based on these performance curves, the CMC and PAM solutions seem to need a certain pressure gradient to initiate flow because they have yield stresses. In particular, the PAM solution needs a higher pressure gradient for flow to start, but the flow rate rapidly

increases because this solution has remarkable shear-thinning properties, as shown in Figure 3b. The performance curve of the porridge is shown in Figure 6b. Similar to the CMC and PAM solutions, this fluid needed a certain pressure gradient for flow to start, following which the flow rate increased nonlinearly with the pressure gradient because of shear thinning. Relative error was calculated at each pressure-gradient condition (see Table 1 in Appendix). The relative

**Table 1. Relative Error  $\epsilon_R$  of Flow Rate at Each Pressure-Gradient Condition  $\alpha$**

| CMC             |                  | PAM             |                  | porridge        |                  |
|-----------------|------------------|-----------------|------------------|-----------------|------------------|
| $\alpha$ [Pa/m] | $\epsilon_R$ [%] | $\alpha$ [Pa/m] | $\epsilon_R$ [%] | $\alpha$ [Pa/m] | $\epsilon_R$ [%] |
| 149             | 3.5              | 229             | −9.3             | 876             | −9.4             |
| 185             | 2.7              | 256             | −1.9             | 1050            | 8.3              |
| 219             | 5.3              | 281             | −5.5             | 1200            | 6.8              |
| 252             | 1.7              | 303             | 2.9              | 1330            | 3.0              |
| 285             | 3.4              | 323             | 5.8              | 1440            | 6.2              |
| 317             | −2.1             | 341             | 3.6              |                 |                  |
| 348             | 4.2              | 357             | −1.6             |                 |                  |

error here is defined as  $\epsilon_R = [(Q_p - Q_e)/Q_e] \times 100\%$ , where  $Q_p$  and  $Q_e$  represent flow rates evaluated in the prediction and experiment, respectively. The maximum relative errors are 5.3% at  $\alpha = 219$  Pa/m for the CMC solution and −9.3% at  $\alpha = 229$  Pa/m for the PAM solution. In the case of the porridge, the maximum relative error is −9.4% at  $\alpha = 876$  Pa/m. Considering that the velocity profiles in the verification experiments were measured by UVP, the precision of which is shown by the error bars in Figure 6, all predictions are considered to fall within acceptable ranges.

Noteworthy here is robustness of the rheological characterization and flow prediction scheme and its high applicability to complex fluids. Multiphase fluids containing  $O(1$  mm) size dispersion, such as the porridge, which can be treated as a continuum approximation for the scale of the UVP measurement volume, are included in the application of this rheological characterization and flow prediction. This proposed methodology does not assume any rheological models based on constitutive equations, so the same protocol can immediately be applied to other complex fluids. Engineers involved in numerical simulations of non-Newtonian fluids may have experienced difficulties in selection of rheological models: flow prediction by utilizing the velocity-profiling-assisted rheometer will be a practical tool for use in industrial fields.

## CONCLUSION

Applicability of a velocity-profiling-assisted rheometer was examined. Silicon oil, a Newtonian fluid, was first measured to validate the rheometer: the result matched the catalog value. Demonstrations of the rheometer were then conducted using carboxymethyl cellulose and polyacrylamide aqueous solutions and rice porridge. The latter two represent complex fluids, which are difficult to evaluate using a standard rheometer because the PAM solution causes shear-localization problems and the porridge includes  $O(1$  mm) size dispersions. Both fluids were evaluated to have a yield stress and remarkable shear-thinning properties. The obtained rheological properties were then applied to predict velocity profiles of the fluids in a circular pipe under a steady pressure gradient. The predictions were in good agreement with experimental results in a pilot pipeline under a range of pressure-gradient conditions. The

velocity profiles were converted to flow rates via an integral operation, and performance curves, which describe the relationship between pressure gradient and flow rate, were obtained for each fluid. The maximum relative error was less than 10% for all test fluids. From the experimental validation, it is concluded that extrapolation from rheological characterization to flow prediction is valid. This velocity-profiling-assisted rheometer has high applicability to complex fluids, such as high-molecular-weight polymer solutions and suspensions containing  $O(1$  mm) size dispersions. This characterization and prediction ability will therefore provide an industrially practical tool.

## APPENDIX

The relative error calculated at each pressure-gradient condition is shown in Table 1 for the CMC and PAM solutions and the rice porridge, respectively.

## AUTHOR INFORMATION

### Corresponding Author

Kohei Ohie – Laboratory for Flow Control, Faculty of Engineering, Hokkaido University, Sapporo 060-8628, Japan; [orcid.org/0000-0002-9137-044X](https://orcid.org/0000-0002-9137-044X); Email: [ohie@ring-me.eng.hokudai.ac.jp](mailto:ohie@ring-me.eng.hokudai.ac.jp)

### Authors

Taiki Yoshida – National Institute of Advanced Industrial Science and Technology, Tsukuba 305-8563, Japan; [orcid.org/0000-0002-9487-6198](https://orcid.org/0000-0002-9487-6198)

Yuji Tasaka – Laboratory for Flow Control, Faculty of Engineering, Hokkaido University, Sapporo 060-8628, Japan; [orcid.org/0000-0002-8943-4803](https://orcid.org/0000-0002-8943-4803)

Yuichi Murai – Laboratory for Flow Control, Faculty of Engineering, Hokkaido University, Sapporo 060-8628, Japan

Complete contact information is available at: <https://pubs.acs.org/10.1021/acs.iecr.2c03022>

### Notes

The authors declare no competing financial interest.

## ACKNOWLEDGMENTS

This work was supported by a Grant-in-Aid for Japan Society for Promotion of Science Fellows (Grant JP22J20991) and Japan Science and Technology Agency PRESTO (Grant JPMJPR2106).

## REFERENCES

- (1) Bird, R. B.; Armstrong, R. C.; Hassager, O. *Dynamics of Polymeric Liquids. Vol. 1: Fluid Mechanics*; Wiley Interscience: New York, 1987.
- (2) Larson, R. G. *The Structure and Rheology of Complex Fluids*; Oxford University Press: New York, 1999.
- (3) Abbasian, M.; Shams, M.; Valizadeh, Z.; Moshfegh, A.; Javadzadegan, A.; Cheng, S. Effects of different non-Newtonian models on unsteady blood flow hemodynamics in patient-specific arterial models with in-vivo validation. *Comput. Methods Programs Biomed.* **2020**, *186*, 105185.
- (4) Warner, H. R., Jr Kinetic theory and rheology of dilute suspensions of finitely extendible dumbbells. *Ind. Eng. Chem. Fundam.* **1972**, *11*, 379–387.
- (5) Fan, X. J. Viscosity, first normal-stress coefficient, and molecular stretching in dilute polymer solutions. *J. Non-Newton. Fluid Mech.* **1985**, *17*, 125–144.

- (6) White, C. M.; Mungal, M. G. Mechanics and prediction of turbulent drag reduction with polymer additives. *Annu. Rev. Fluid Mech.* **2008**, *40*, 235–256.
- (7) Alves, M.; Oliveira, P.; Pinho, F. Numerical methods for viscoelastic fluid flows. *Annu. Rev. Fluid Mech.* **2021**, *53*, 509–541.
- (8) Macosko, C. W. *Rheology Principles, Measurements, and Applications*; VCH: New York, 1994.
- (9) Irgens, F. *Rheology and Non-Newtonian Fluids*; Springer: Germany, 2014.
- (10) Fischer, P.; Wheeler, E. K.; Fuller, G. G. Shear-banding structure orientated in the vorticity direction observed for equimolar micellar solution. *Rheol. Acta* **2002**, *41*, 35–44.
- (11) Sui, C.; McKenna, G. B. Instability of entangled polymers in cone and plate rheometry. *Rheol. Acta* **2007**, *46*, 877–888.
- (12) Fardin, M. A.; Perge, C.; Casanellas, L.; Hollis, T.; Taberlet, N.; Ortin, J.; Lerouge, S.; Manneville, S. Flow instabilities in large amplitude oscillatory shear: a cautionary tale. *Rheol. Acta* **2014**, *53*, 885–898.
- (13) Divoux, T.; Fardin, M. A.; Manneville, S.; Lerouge, S. Shear banding of complex fluids. *Annu. Rev. Fluid Mech.* **2016**, *48*, 81–103.
- (14) de Souza Mendes, P. R.; Aliche, A. A.; Thompson, R. L. Parallel-plate geometry correction for transient rheometric experiments. *Appl. Rheol.* **2014**, *24*, 52721.
- (15) Saint-Michel, B.; Gibaud, T.; Leocmach, M.; Manneville, S. Local oscillatory rheology from echography. *Phys. Rev. Appl.* **2016**, *5*, 034014.
- (16) Yoshida, T.; Tasaka, Y.; Fischer, P. Ultrasonic spinning rheometry test on the rheology of gelled food for making better tasting desserts. *Phys. Fluids* **2019**, *31*, 113101.
- (17) Rust, A.; Manga, M. Effects of bubble deformation on the viscosity of dilute suspensions. *J. Non-Newton. Fluid Mech.* **2002**, *104*, 53–63.
- (18) Llewellyn, E.; Mader, H.; Wilson, S. The rheology of a bubbly liquid. *Proc. R. Soc. A: Math. Phys. Eng. Sci.* **2002**, *458*, 987–1016.
- (19) Mueller, S.; Llewellyn, E.; Mader, H. The rheology of suspensions of solid particles. *Proc. R. Soc. A: Math. Phys. Eng. Sci.* **2010**, *466*, 1201–1228.
- (20) Mader, H.; Llewellyn, E.; Mueller, S. The rheology of two-phase magmas: A review and analysis. *J. Volcanol. Geotherm. Res.* **2013**, *257*, 135–158.
- (21) Derakhshandeh, B.; Vlassopoulos, D.; Hatzikiriakos, S. G. Thixotropy, yielding and ultrasonic Doppler velocimetry in pulp fibre suspensions. *Rheol. Acta* **2012**, *51*, 201–214.
- (22) Takeda, Y. Velocity profile measurement by ultrasonic Doppler method. *Exp. Therm. Fluid Sci.* **1995**, *10*, 444–453.
- (23) Takeda, Y. *Ultrasonic Doppler Velocity Profiler for Fluid Flow*; Springer: Germany, 2012.
- (24) Yoshida, T.; Tasaka, Y.; Murai, Y. Rheological evaluation of complex fluids using ultrasonic spinning rheometry in an open container. *J. Rheol.* **2017**, *61*, 537–549.
- (25) Shiratori, T.; Tasaka, Y.; Oishi, Y.; Murai, Y. Ultrasonic velocity profiling rheometry based on a widened circular Couette flow. *Meas. Sci. Technol.* **2015**, *26*, 085302.
- (26) Shiratori, T.; Tasaka, Y.; Murai, Y. Rapid rheological characterization of a viscoelastic fluid based on spatiotemporal flow velocimetry. *Exp. Therm. Fluid Sci.* **2016**, *71*, 1–13.
- (27) Kulicke, W. M.; Kull, A. H.; Kull, W.; Thielking, H.; Engelhardt, J.; Pannek, J.-B. Characterization of aqueous carboxymethylcellulose solutions in terms of their molecular structure and its influence on rheological behaviour. *Polymer* **1996**, *37*, 2723–2731.
- (28) Ghannam, M. T.; Esmail, M. N. Rheological properties of carboxymethyl cellulose. *J. Appl. Polym. Sci.* **1997**, *64*, 289–301.
- (29) Benchabane, A.; Bekkour, K. Rheological properties of carboxymethyl cellulose (CMC) solutions. *Colloid Polym. Sci.* **2008**, *286*, 1173–1180.
- (30) Ghannam, M. T.; Esmail, M. N. Rheological properties of aqueous polyacrylamide solutions. *J. Appl. Polym. Sci.* **1998**, *69*, 1587–1597.
- (31) Lewandowska, K. Comparative studies of rheological properties of polyacrylamide and partially hydrolyzed polyacrylamide solutions. *J. Appl. Polym. Sci.* **2007**, *103*, 2235–2241.
- (32) Ohie, K.; Yoshida, T.; Tasaka, Y.; Murai, Y. Effective rheology mapping for characterizing polymer solutions utilizing ultrasonic spinning rheometry. *Exp. Fluids* **2022**, *63*, 40.
- (33) Andereck, C. D.; Liu, S.; Swinney, H. L. Flow regimes in a circular Couette system with independently rotating cylinders. *J. Fluid Mech.* **1986**, *164*, 155–183.
- (34) González, H. A.; Moraga, N. O. On predicting unsteady non-Newtonian blood flow. *Appl. Math. Comput.* **2005**, *170*, 909–923.
- (35) Poole, R.; Ridley, B. Development-length requirements for fully developed laminar pipe flow of inelastic non-Newtonian liquids. *J. Fluids Eng.* **2007**, *129*, 1281–1287.
- (36) Tasaka, Y.; Yoshida, T.; Murai, Y. Nonintrusive in-line rheometry using ultrasonic velocity profiling. *Ind. Eng. Chem. Res.* **2021**, *60*, 11535–11543.
- (37) Ouriev, B.; Windhab, E. Rheological study of concentrated suspensions in pressure-driven shear flow using a novel in-line ultrasound Doppler method. *Exp. Fluids* **2002**, *32*, 204–211.
- (38) Wiklund, J.; Shahram, I.; Stading, M. Methodology for in-line rheology by ultrasound Doppler velocity profiling and pressure difference techniques. *Chem. Eng. Sci.* **2007**, *62*, 4277–4293.

## Recommended by ACS

### Effect of Bend on Film Thickness in Slug, Slug-Annular, and Annular Flow Regimes in Gas-Liquid Flow in a Microchannel

Deepak Kumar Mishra, Anugrah Singh, et al.

SEPTEMBER 08, 2022

INDUSTRIAL & ENGINEERING CHEMISTRY RESEARCH

READ 

### Commentary: Evolution of High Gravity (HiGee) Technology

D. P. Rao.

JANUARY 06, 2022

INDUSTRIAL & ENGINEERING CHEMISTRY RESEARCH

READ 

### Multiphase Flow Characteristics in the Classification Process of a Novel Wide Neck Thickeners: Experiment and Simulation

Yan Zheng, Chuanzhen Wang, et al.

OCTOBER 17, 2022

ACS OMEGA

READ 

### Numerical Simulations of Solidification Characteristics of Molten Slag Droplets in Radiant Syngas Coolers for Entrained-Flow Coal Gasification

Bo Wang, Guangsuo Yu, et al.

JULY 27, 2021

ACS OMEGA

READ 

Get More Suggestions >